Proceedings of the 21st ICSMGE, Vienna, Austria, 14 – 19 June 2026. Pistrol, Adam & Schweiger (eds.)
Published by: ÖGG, Austrian Society for Geomechanics, Salzburg, Austria, ISBN 978-3-9503898-4-5
https://doi.org/10.53243/ICSMGE2026-679

GPU-Parallelized HFDEM simulation of calcareous sand particle crushing based on Micro-CT mesh reconstruction

Fei Liu
Department of Infrastructure Engineering, University of Melbourne, Melbourne, Australia

Hongyuan Liu
School of Engineering, University of Tasmania, Hobart, Australia

Jay Black
School of Earth Sciences, University of Melbourne, Melbourne, Australia

Yinghui Tian
Department of Infrastructure Engineering, University of Melbourne, Melbourne, Australia, yinghui.tian@unimelb.edu.au

ABSTRACT: The hybrid finite–discrete element method (HFDEM) has proven its high effectiveness in simulating rock fracture and soil mechanics at macro scales. This study extends HFDEM to microscopic scale to simulate the crushing of calcareous sand particles. Based on high-resolution micro-CT imaging (25 μm), complex particle geometries were meshing with over 225,000 tetrahedral elements. The cohesive element formulation within HFDEM enables an accurate simulation of the transition from continuum deformation to discrete fracturing, allowing modelling the complete crushing process of the highly porous grains of calcareous sand. The HFDEM modelling results demonstrate a brittle crushing behavior for calcareous sand, featured with an initial elastic response, crack initiation at contact points, propagation through porous structures, and final progressive fragmentation. Internal porosity is shown to affect fracture evolution, with stress concentrations forming along pore boundaries and eventually leading to preferential cracking. A peak crushing force of 212 N occurs at 0.30 mm displacement for a particle with a maximum dimension of 17 mm, followed by 85% strength loss due to multiple fracture events. These findings demonstrate HFDEM offers a promising approach to investigate the crushing mechanisms of calcareous sand and its potential to bridge up macro-scale geotechnical behavior.

KEYWORDS: HFDEM, Micro-CT imaging, single particle crushing, calcareous sand, particle-scale mechanics.

1 INTRODUCTION

The combined finite–discrete element method (FDEM) has emerged as a powerful numerical tool in geotechnical and rock engineering, demonstrating exceptional capabilities in simulating large-scale failure processes. Originally proposed by Munjiza et al. (1995), FDEM's unique ability to capture the complete transition from continuum deformation to discontinuous fracture within a unified framework has been extensively validated across various engineering problems, including slope instability (An et al., 2022), tunnel collapse (Han et al., 2020), blast-induced fracturing (An et al., 2021; Liu et al., 2021) and rock failure (Fukuda et al., 2021; Wu et al., 2022). These applications highlight the method's capability to handle problems involving large deformations, fracture propagation, and fragmentation in both soils and rocks under diverse loading and boundary conditions. While these large-scale applications have been extensively validated, extending HFDEM to microscopic particle breakage presents unique challenges due to geometric complexity, mechanical nonlinearity, and high computational demands (Li et al., 2023).

Calcareous sand represents a particularly challenge among a range of geomaterials. These biogenic sediments, prevalent in offshore regions including north-west shelf of Australia, the South China Sea, and the Middle East (Gao & Ye, 2023), can present critical difficulties for marine infrastructure development. Their biological origin results in irregular morphologies, extensive internal porosity, and significantly lower particle strength compared to siliceous sands (Xu et al., 2022), making them highly susceptible to crushing (Lv et al., 2024). Understanding these particle-scale breakage mechanisms is essential for predicting the macro-scale performance of marine foundations.

As shown in Figure 1, the particles manifest complex pore networks extending from the particle surface deep into the interior. Such features are liable for substantial particle crushing under engineering level loads, directly influencing macro-scale properties (Wu et al., 2022), bearing capacity (Coop, 1990), and long-term settlement performance (He et al., 2020).

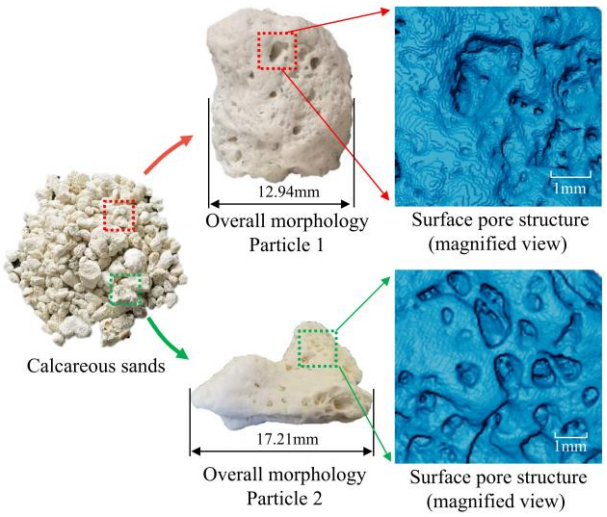

Figure 1. Morphological characteristics of calcareous sand particles.

Despite experimental investigations using single particle compression tests and CT imaging, numerical studies capturing the complete fracture process remain limited (Li et al., 2025). The hybrid finite-discrete element method (HFDEM), developed by Liu et al., (2015), incorporates advanced features including GPGPU parallelization and adaptive contact algorithms, achieving computational efficiency improvements of 8,000-61,000 times compared to sequential implementations (Fukuda et al., 2021). This study applies the HFDEM to simulate single calcareous sand particle crushing, based on

mesh constructed from Micro-CT scanning to reveal crack evolution patterns, identify critical breakage stresses, and provide fundamental insights in calcareous deposits.

2 HFDEM METHOD AND RECENT ADVANCES

2.1 *Basic Principle*

The hybrid finite-discrete element method (HFDEM) combines the strengths of finite element methods (FEM) in capturing continuum deformation and discrete element methods (DEM) in simulating discontinuous fracture and contact behavior. As illustrated in Figure 2, cohesive elements inserted between finite elements allow for the simulation of tensile and shear softening, enabling realistic modeling of crack initiation, propagation, and coalescence within individual particles (Liu et al., 2015).

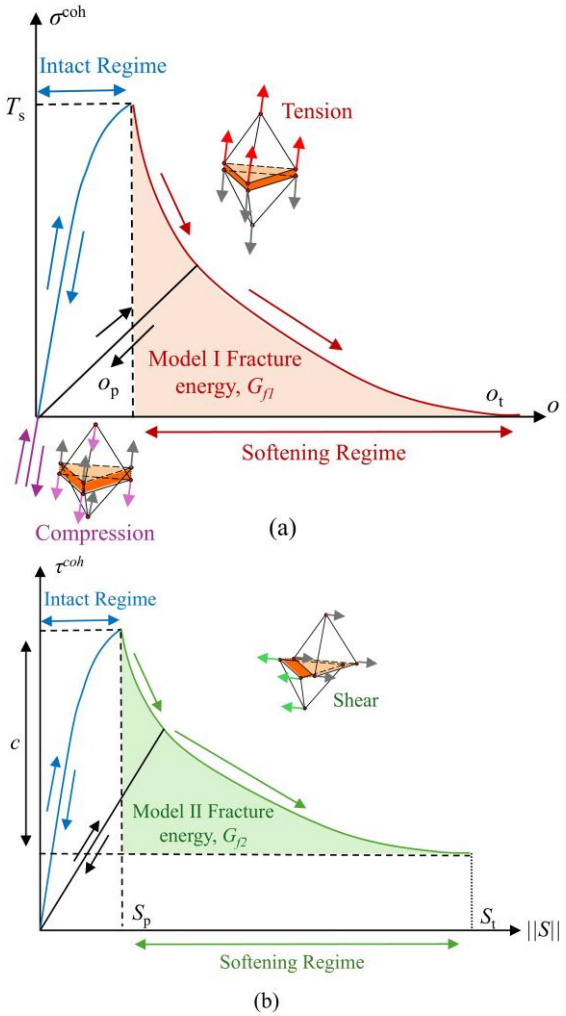

Figure 2. Constitutive behaviors of cohesive elements: (a) Mode I tensile failure with traction-separation law; (b) Mode II shear failure with traction-separation law.

In HFDEM, the normal cohesive traction σ^{coh} is computed based on the opening displacement o and damage state:

$$\sigma^{coh} = \begin{cases} \dfrac{2o}{o_{overlap}} T_s, & o < 0 \\ \left[\dfrac{2o}{o_p} - \left(\dfrac{o}{o_p}\right)^2\right] f(D) T_s, & 0 \le o \le o_p \\ f(D) T_s, & o > o_p \end{cases} \quad (1)$$

Where T_s is the tensile strength, o_p is the elastic limit for opening displacement, $o_{overlap}$ is the representative overlap when o is negative.

The shear cohesive traction τ^{coh} incorporates the Mohr-Coulomb failure criterion with tension cut-off:

$$\tau^{coh} = \begin{cases} \left[\dfrac{2s}{s_p} - \left(\dfrac{|s|}{s_p}\right)^2\right] [f(D)c - \sigma^{coh} tan\emptyset], & 0 \le |s| \le s_p \\ f(D)c - \sigma^{coh} tan\emptyset, & s_p < |s| \end{cases} \quad (2)$$

Where s is the shear displacement, s_p is the elastic limit of shear displacement, $\emptyset$ is the internal friction angle, c is the cohesion.

Opening displacement o and tensile stress σ^{coh} become positive during crack formation. The $f(D)$ function governs strength reduction as fractures develop. Once elements enter the softening regime beyond o_p (or s_p), damage accumulation becomes irreversible even upon unloading. Complete separation occurs when thresholds ($o \ge o_t$, $\|s\| \ge s_t$) are exceeded, after which interaction is governed by contact mechanics only.

2.2 *Computational Enhancements*

To address the intensive computational requirements for contact detection and fracture modeling in irregular particles, significant advances have been implemented in the GPGPU-parallelized HFDEM code. The computational efficiency improvements include GPGPU parallelization using CUDA C/C++, achieving speedups of 8,000–61,000 times compared to sequential implementations (Fukuda et al., 2021).

Dynamic equilibrium is achieved through local damping with mass scaling:

$$\boldsymbol{M}^{scale} \frac{\partial^2 \boldsymbol{u}}{\partial t^2} = \boldsymbol{f}_{tot} + \alpha \|\boldsymbol{f}_{tot}\| sgn(v) \quad (3)$$

Where $\boldsymbol{M}^{scale}$ signifies the scaled concentrated mass matrix, $\boldsymbol{f}_{tot}$ refers to the unbalanced nodal force vector, $\|\boldsymbol{f}_{tot}\|$ expresses the absolute value magnitude for individual components of $\boldsymbol{f}_{tot}$, v stands for nodal velocity values, sgn(·) functions as the mathematical sign operator, while α characterizes the localized damping coefficient.

Additional computational strategies include adaptive contact activation that restricts calculations to boundary elements and newly failed regions, semi-adaptive contact activation to prevent spurious fracture modes under shear softening, hyperplane separation theorem for efficient contact detection, and mass scaling techniques enabling larger stable time steps (Liu & Fukuda, 2022). These enhancements collectively enable efficient simulation of complex particle breakages involving thousands of irregular-shaped fragments.

3 APPLICATION TO CALCAREOUS SAND PARTICLES

3.1 *Particle Selection and Imaging*

Individual calcareous sand particles ranging from 1–5 cm in diameter were isolated and prepared for high-resolution imaging. Micro-computed tomography (μCT) scanning was performed using the Phoenix Nanotom M scanner (Waygate Technologies) at the University of Melbourne (Tee et al., 2023) with a scanning accuracy of 25 microns, providing sufficient resolution for detailed characterization of both external morphology and internal pore networks. Figure 3 illustrates the complete workflow from bulk sample selection to CT acquisition.

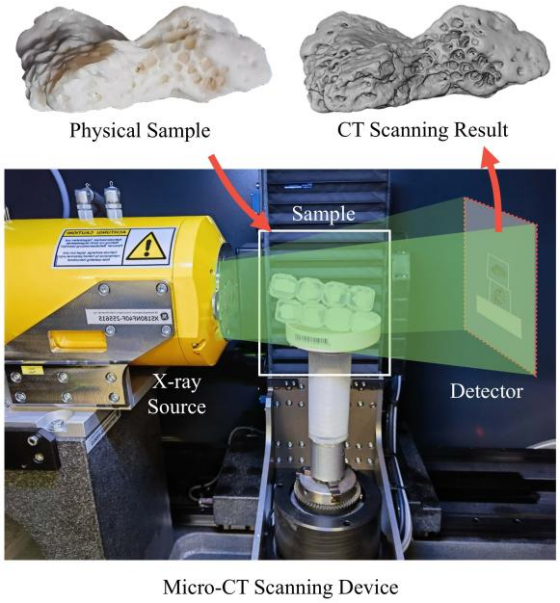

Figure 3. Physical sample and CT scanning result of calcareous sand.

3.2 *Mesh Generation for HFDEM Analysis*

The μCT tiff stack datasets were converted into computational meshes through systematic image processing. Image enhancement included ring artifact removal, intensity bias correction, and contrast enhancement (Schlüter et al., 2014). Threshold-based segmentation distinguishes solid material from voids, followed by morphological filtering to remove noise and isolated pixels.

Tetrahedral mesh generation used Delaunay triangulation with a minimum element size of 0.1 mm, balancing computational efficiency with morphological detail capture. Mesh quality control included automatic repair, aspect ratio checks, and degenerate element removal. Figure 4 demonstrates the complete processing workflow for a representative calcareous sand particle, resulting in a mesh containing 225,537 tetrahedral elements and 485,580 surface nodes.

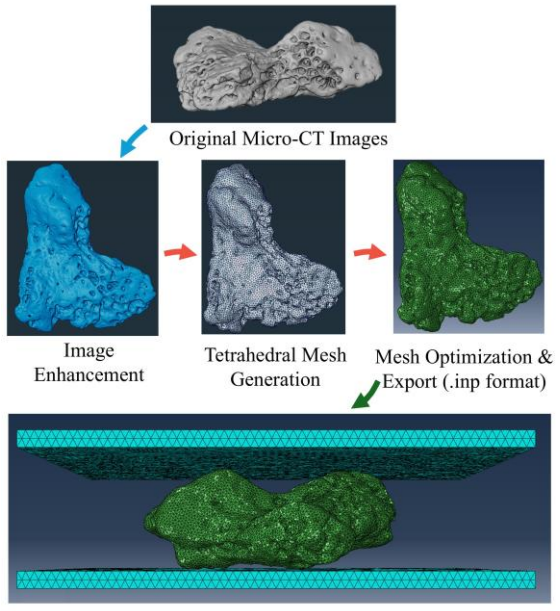

Figure 4. Micro-CT image processing and mesh generation workflow for HFDEM simulation.

Material parameters are summarized in Table 1, reflecting typical calcareous sand properties with relatively low tensile and shear strengths. Lower cohesive element fracture energies (GI = 0.30 N/mm, GII = 0.20 N/mm) were deliberately chosen to enhance crack propagation visualization and fragmentation behavior. While detailed parameter calibration is beyond this study's scope, the selected values effectively demonstrate the fracture evolution patterns under investigation.

Table 1. Calibrated parameters in HFDEM simulation.

Category	Parameters	Symbol	Value
Particle elements	Density	ρ	2700kg/m^3
	Young's modulus	E	20 GPa
	Poisson's ratio	N	0.32
	Coefficient of friction	μ_s	0.5
Cohesive element	Normal stiffness	k_n	5000 N/mm^3
	Shear stiffness	k_s	4000 N/mm^3
	Tensile strength	f_n	15 MPa
	Shear strength	f_s	10 MPa
	Tensile fracture energy	G_I	0.30 N/mm
	Shear fracture energy	G_{II}	0.20 N/mm
Loading Platen	Coefficient of friction	μ_R	0.05
	Loading rate	v	0.1 m/s

3.3 *Simulation Setup and Computational Details*

The single particle crushing simulation employed uniaxial compression between two rigid plates. The bottom platen remained fixed, while the top platen moved downward at a constant velocity of 0.1 m/s. This loading rate was chosen to balance fracture pattern clarity and computational efficiency, noting this analysis is a quasi-static process. The particle was oriented with its longest axis approximately perpendicular to the loading direction to maximize contact stability.

Automatic critical damping combined with viscous damping was utilized to mitigate dynamic effects and approximate quasi-static conditions. An explicit time integration scheme with adaptive time stepping ensured numerical stability throughout the crushing process. The simulation continued until complete particle fragmentation occurred.

4 SINGLE PARTICLE BREAKAGE ANALYSIS

4.1 *Crack Propagation Evolution*

Figure 5 illustrates the front and side section planes that serve as reference orientations for multi-view observation of the particle crushing process.

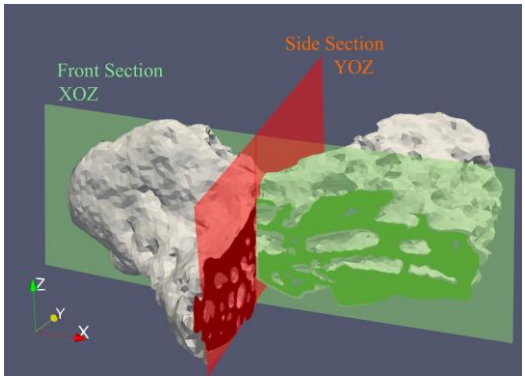

Figure 5. Section planes for multi-view analysis.

Figure 6 presents the progressive crushing behavior of a calcareous sand particle under uniaxial compression at four simulation time steps: 20 ms, 30 ms, 50 ms, and 70 ms. Using the section orientations illustrated in Figure 5, subfigures (a)–(c) in Figure 6 show Z-directional stress distributions from different perspectives (front view, front section XOZ, side section YOZ), while subfigures (d) depict fully fractured cohesive elements, representing the spatial evolution of cracking.

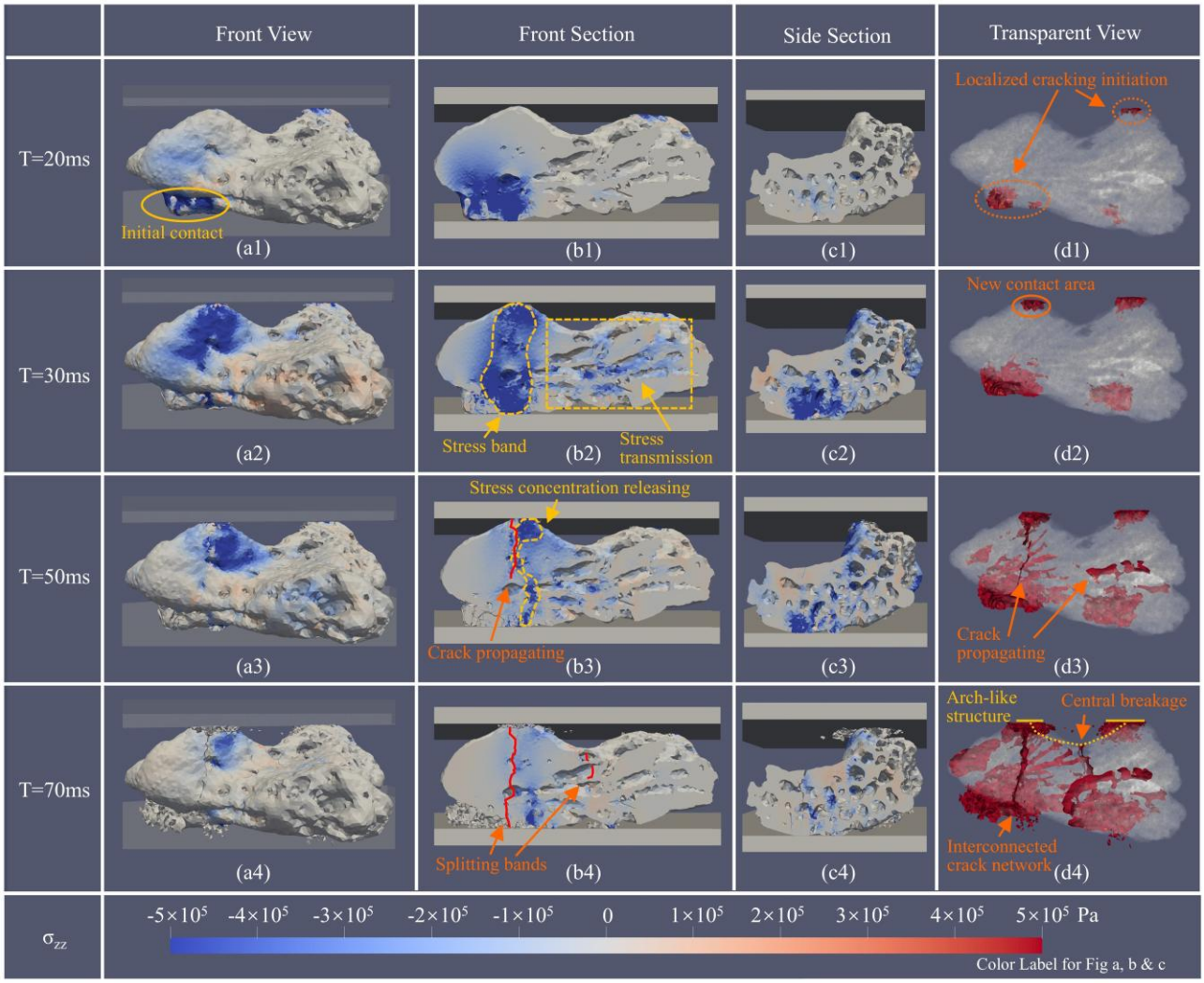

Figure 6. Progressive crushing of a calcareous sand particle under uniaxial compression at T = 20, 30, 50, and 70 ms: (a) front view, (b) front section, (c) side section, and (d) internal crack evolution.

At 20 ms, the upper platen makes initial contact with the particle. Stress concentrations are observed at the top and bottom contact areas, indicated by intense red and blue zones near the loading boundaries. Correspondingly, localized cracking initiates in these zones, as shown in Figure 6(d1).

By 30 ms, additional contact is established on the elevated ridge at the particle's left side. A clear stress band emerges from the left-top contact point to the lower-left base, following the internal pore structure. Stress transmission is also evident along adjacent pores. Figure 6(d2) illustrates the expansion of damage zones, notably the appearance of a new crack near the upper-left region, increasing the number of active breakage sites.

At 50 ms, stress concentration in the previously loaded area diminishes, indicating energy release through fracture. Multiple cracks propagate through the porous structure, forming splitting patterns. A prominent vertical crack emerges from the lower-left breakage zone, guided by internal pore weaknesses. Meanwhile, a new central crack starts to develop, as seen in Figure 6(d3).

By 70 ms, crack coalescence forms major splitting bands throughout the particle. The central region exhibits significant fragmentation. The development of an arch-like structure between the two upper contact zones results in stress accumulation from opposing directions, accelerating internal failure. Figure 6(d4) reveals a more extensive and interconnected crack network, confirming the culmination of particle breakage.

These results demonstrate the capability of HFDEM in capturing stress redistribution, pore-induced crack guidance, and progressive fragmentation in calcareous sand grains, offering fundamental insights into micro-scale failure mechanisms.

4.2 *Mechanical Response*

Figure 7 presents the force–displacement response of a calcareous sand particle under uniaxial compression, with overlaid snapshots illustrating the crack evolution at representative stages. The curve reveals characteristic features of brittle particle crushing, segmented into distinct mechanical phases.

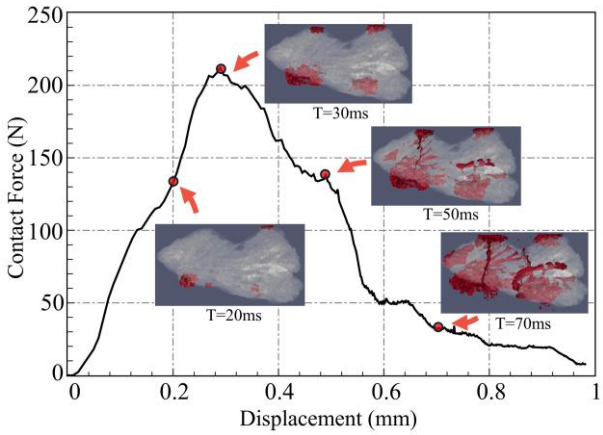

Figure 7. Force–displacement curve of a calcareous sand particle under uniaxial compression with representative crack evolution snapshots.

In the initial stage (0–0.2 mm displacement), the force rises nonlinearly to approximately 200 N, reflecting gradual contact formation between the irregular particle surface and the loading platen. This is followed by a quasi-linear segment (0.2–0.3 mm), indicating elastic deformation with increasing contact stiffness.

The peak force of approximately 212 N occurs at a displacement of 0.30 mm, marking the onset of unstable crack propagation. A significant force drop—about 35% to 130 N—is observed between 0.30–0.50 mm, corresponding to the rapid development of splitting cracks through the porous interior, as depicted in the crack overlay.

A second major force reduction occurs between 0.50–0.60 mm, dropping from 130 N to approximately 60 N, indicating the formation of a primary splitting plane that effectively divides the particle into major fragments. This critical failure event is clearly visible in the crack evolution at T=50ms.

The post-peak stage (0.60–1.0 mm) is characterized by gradual force degradation with smaller intermittent drops, each associated with secondary fragmentation and crack coalescence. By 1.0 mm, the residual force stabilizes at approximately 30 N, retaining only ~15% of the peak strength. This correlates with extensive structural disintegration shown in the final image.

Overall, the force–displacement behavior reflects the typical crushing response of highly porous particles: an initial nonlinear contact phase, brittle peak failure, and gradual post-peak softening via successive fracture events. The area under the curve represents the energy dissipated through particle crushing, indicative of the particle's fracture toughness and internal heterogeneity.

5 CONCLUSIONS

This study demonstrates the applicability of the hybrid finite–discrete element method (HFDEM) in simulating the crushing of calcareous sand particles under uniaxial compression. The key findings are as follows:

- HFDEM effectively captures the complete fracture process of porous particles, including crack initiation, propagation, and coalescence, through cohesive element modeling with GPU-based computational acceleration.
- μCT-based geometry integration enables realistic particle morphology representation, revealing how internal pore structures fundamentally control crack evolution pathways and the formation of failure planes.
- The mechanical response exhibits typical brittle crushing characteristics: nonlinear contact establishment, catastrophic failure at peak load, and gradual post-peak softening through progressive fragmentation. The observed fracture energy dissipation directly reflects the particle's microstructural complexity and heterogeneity.

These insights contribute to understanding calcareous sand behavior at the particle scale and provide a validated numerical framework for investigating marine geomaterials. Future work will explore the relationship between particle morphology and crushing behavior, as well as inter-particle contact mechanisms in multi-particle systems.

6 ACKNOWLEDGEMENTS

The first author gratefully acknowledges the financial support from the China Scholarship Council–The University of Melbourne Scholarship Program (CSC, Grant No. 202308130052). This study was undertaken with support from Australian Research Council (ARC) Discovery Projects (DP250101149). The corresponding author acknowledges the ARC Future Fellowship (FT200100457) to support his research in offshore geotechnics.

7 REFERENCES

An, H., Fan, Y., Liu, H., Cheng, Y. and Song, Y. 2022. The State of the Art and New Insight into Combined Finite–Discrete Element Modelling of the Entire Rock Slope Failure Process. *Sustainability* 14(9), 4896.

An, H., Song, Y., Liu, H. and Han, H. 2021. Combined Finite-Discrete Element Modelling of Dynamic Rock Fracture and Fragmentation during Mining Production Process by Blast. *Shock and Vibration* 2021, 1–18.

Coop, M.R. 1990. The mechanics of uncemented carbonate sands. *Géotechnique* 40(4), 607–626.

Fukuda, D., Liu, H., Zhang, Q., Zhao, J., Kodama, J., Fujii, Y. and Chan, A.H.C. 2021. Modelling of dynamic rock fracture process using the finite-discrete element method with a novel and efficient contact activation scheme. *International Journal of Rock Mechanics and Mining Sciences* 138, 104645.

Gao, R. and Ye, J. 2023. Mechanical behaviors of coral sand and relationship between particle breakage and plastic work. *Engineering Geology* 316, 107063.

Han, H., Fukuda, D., Liu, H., Salmi, E.F., Sellers, E., Liu, T. and Chan, A. 2020. Combined finite-discrete element modelling of rock fracture and fragmentation induced by contour blasting during tunnelling with high horizontal in-situ stress. *International Journal of Rock Mechanics and Mining Sciences* 127, 104214.

He, S.-H., Ding, Z., Xia, T.-D., Zhou, W.-H., Gan, X.-L., Chen, Y.-Z. and Xia, F. 2020. Long-term behaviour and degradation of calcareous sand under cyclic loading. *Engineering Geology* 276, 105756.

Li, X., Lv, Y., Su, Y., Zou, K., Wang, Y. and Huang, W. 2023. Coupling effects of morphology and inner pore distribution on the mechanical response of calcareous sand particles. *Journal of Rock Mechanics and Geotechnical Engineering* 15(6), 1565–1579.

Li, Z., Zhang, Y., Chen, R., Tai, P. and Zhang, Z. 2025. Numerical investigation of morphological effects on crushing characteristics of single calcareous sand particle by finite-discrete element method. *Powder Technology* 453, 120592.

Liu, H. and Fukuda, D. 2022. Development and application of a GPGPU-parallelized hybrid finite-discrete element method for modelling geo-structure collapse and resultant debris flow. *Proc. 20th International Conference on Soil Mechanics and Geotechnical Engineering*, Sydney, 815–820.

Liu, H., Fukuda, D. and Han, H. 2021. Development and application of a three-dimensional GPGPU-parallelized FDEM for modelling rock fragmentation by blast. *IOP Conference Series: Earth and Environmental Science* 861(3), 032027.

Liu, H.Y., Kang, Y.M. and Lin, P. 2015. Hybrid finite–discrete element modeling of geomaterials fracture and fragment muck-piling. *International Journal of Geotechnical Engineering* 9(2), 115–131.

Lv, Y., Hu, J., Zhang, D., Wang, Y. and Su, Y. 2024. Particle breakage of calcareous sand from low-high strain rates. *Journal of Rock Mechanics and Geotechnical Engineering* 16(12), 5249–5263.

Munjiza, A., Owen, D.R.J. and Bicanic, N. 1995. A combined finite-discrete element method in transient dynamics of fracturing solids. *Engineering Computations* 12(2), 145–174.

Schlüter, S., Sheppard, A., Brown, K. and Wildenschild, D. 2014. Image processing of multiphase images obtained via X-ray microtomography: A review. *Water Resources Research* 50, 3615–3639.

Tee, Y.L., Black, J.R. and Tran, P. 2023. Virtual characterisation of porcupine quills using X-ray micro-CT. *Virtual and Physical Prototyping* 18(1), e2126377.

Wu, Y., Wu, Y., Liu, J., Li, N. and Li, S. 2022. The evolution and influence of particle breakage on the compression behavior of calcareous sand. *Marine Georesources & Geotechnology* 40(6), 668–678.

Xu, L.-J., Wang, X., Wang, R., Zhu, C. and Liu, X. 2022. Physical and mechanical properties of calcareous soils: A review. *Marine Georesources & Geotechnology* 40(6), 751–766.